A Femtosecond Code-Division Multiple-Access Communication System Test Bed

H. P. Sardesai, C.-C. Chang, and A. M. Weiner

***Abstract*—This paper reports comprehensive experimental results on a femtosecond code-division multiple-access (CDMA) communication system test bed operating over optical fiber in the 1.5 μm communication band. Our test bed integrates together several novel subsystems, including low-loss fiber-pigtailed pulse shapers for encoding–decoding, use of dispersion equalizing fibers in dispersion compensated links for femtosecond pulse transmission and also in femtosecond chirped pulse amplification (CPA) erbium doped fiber amplifiers (EDFA's), and high-contrast nonlinear fiber-optic thresholders. The individual subsystems are described, and single-user system level experimental results demonstrating the ability to transmit spectrally encoded femtosecond pulses over a 2.5-km dispersion compensated fiber link followed by decoding and high contrast nonlinear thresholding are presented.**

***Index Terms*— CDMA, dispersion compensation, nonlinear thresholding, pulse-shaping, ultrafast phenomena.**

I. Introduction

TO meet the demand for high-speed and high-capacity communications, multiple-access schemes are necessary which allow multiple users to access the network simultaneously by sharing the same fiber-optic transmission medium. For long distance communication, wavelength division multiplexing (WDM) and time-division multiplexing (TDM) have been extensively explored and have shown impressive performance results [1]–[6]. For local area network (LAN) applications, optical code-division multiple-access (CDMA) communications systems [7]–[20] are also being investigated, in addition to the more traditional WDM and TDM schemes. Each data bit in an optical CDMA system is coded with a code that is unique to a particular user, and multiple users are accommodated by assigning different minimally interfering codes to different user pairs. Several different minimally correlated code-sequences exist in traditional digital communication systems that can be implemented in the optical domain making optical CDMA suitable for multi-user operation, the main constraints being the fidelity of the encoding–decoding operation for a user pair and the consequent successful detection in the presence of interference from other users. CDMA is well suited for bursty network environments, and optical CDMA has the advantage of using optical processing to perform certain network applications like addressing and routing. The asynchronous nature of data transmission can simplify network management and control. Hence, due to the advantages of optical processing, asynchronous transmission, and the capability of multiple-access in a bursty environment, optical CDMA appears to be an interesting possibility for LAN applications. On the other hand, the technologies required for implementing optical CDMA systems are significantly less mature and may be inherently more complex than those required for TDM or especially WDM systems.

Several different optical CDMA schemes have been proposed [7]–[20], based on different choices of sources, coding schemes and detection. Two reviews of optical CDMA are given in [14] and [15]. Optical CDMA schemes may be classified according to the choice of coherent versus incoherent processing, coherent (modelocked pulses) versus incoherent (e.g., amplified spontaneous emission) broadband optical source, and encoding method (time-domain versus frequency-domain, amplitude versus phase). Schemes based on incoherent processing (summing of optical *powers*) and broadband incoherent (noise) sources are generally the easiest to implement. However, as in radio spread spectrum, coherent processing based on manipulation of optical *fields*, which can be made to sum to zero, is needed for good suppression of multiple-access interference. Note that coherent processing is possible even for systems using incoherent noise sources, e.g., coherence multiplexing approaches based on interferometric techniques; however, recent analyzes have shown that optical beat noise becomes a major factor limiting the capacity of such systems [14]. Here, we experimentally investigate an ultrashort pulse optical CDMA scheme based on spectral phase encoding and decoding of coherent modelocked pulses [7], [15]. Note that for ultrashort pulse CDMA, multiple-access crosstalk and optical beat noise are essentially synonymous. A theoretical analysis of the cross-talk limited performance of this approach indicates the potential for CDMA systems with capacities from tens to perhaps (100 Gb/s, depending on how short a pulse width and how long a code length can be maintained during system operation [7], [15].

A block diagram of the ultrashort pulse CDMA scheme configured for LAN applications is shown in Fig. 1. In the transmitter, femtosecond laser pulses are spectrally encoded by a pseudorandom phase code that transforms the femtosecond pulses into picosecond duration pseudonoise signals. Each user

Manuscript received November 20, 1997; revised July 10, 1998. This work was supported by the National Science Foundation under Grants ECS-96 26967 and ECS-9312256.

H. P. Sardesai was with the School of Electrical and Computer Engineering, Purdue University, West Lafayette, IN 47907 USA. He is now with Ciena Corporation, Linthicum, MD 21090 USA.

C.-C. Chang was with the School of Electrical and Computer Engineering, Purdue University, West Lafayette, IN 47907 USA. He is now with Bell Laboratories, Lucent Technologies, Holmdel, NJ 07733 USA.

A. M. Weiner is with the School of Electrical and Computer Engineering, Purdue University, West Lafayette, IN 47907 USA.

Publisher Item Identifier S 0733-8724(98)08307-8.

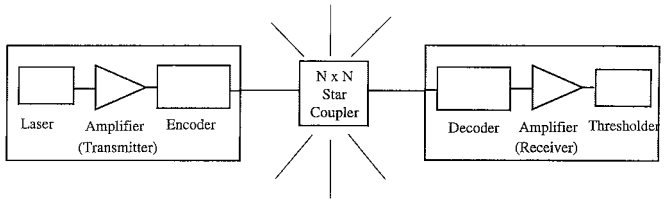

Fig. 1. Block diagram of the femtosecond CDMA test bed.

(transmitter) is assigned a unique phase code by which it encodes all its data bits, and this phase code is chosen to be minimally interfering compared to the phase codes assigned to every other user in the system. Different users can be connected in a simple broadcast and select type architecture where all transmitters are connected to all receivers by a passive star coupler. Each receiver thus receives encoded data bits transmitted by every transmitter in the network, but the decoder in any one receiver matches the phase code of only one transmitter. Hence, only the encoded data bits of one transmitter that are intended for a particular receiver get properly decoded back to a femtosecond pulse, and the encoded data bits transmitted by all other transmitters remain as improperly decoded pseudonoise signals. A nonlinear fiber-optic thresholder then performs the task of distinguishing between the correctly decoded femtosecond signal and the incorrectly decoded picosecond interference. In this CDMA scheme, each transmitter may operate at moderate data rates (e.g., on the order of 1 Gb/s), but with multiple-access higher overall data transmission rates may be achieved.

In this paper we demonstrate for the first time to our knowledge that all the operations required for femtosecond pulse CDMA, namely spectral encoding, fiber transmission with dispersion compensation, spectral decoding, and nonlinear optical thresholding, can be accomplished with good fidelity in an integrated system. Some of our preliminary results were described earlier [20]. In the course of constructing an ultrashort pulse CDMA "test bed," we have developed several ultrashort pulse CDMA component and subsystem technologies that may also have broader application to ultrafast optical communications and have begun to assess component technology limitations that may impact overall system performance. Note that in our optical CDMA test bed we currently demonstrate single-user operation consisting of one transmitter and one receiver. We currently encode every laser pulse, although a real system would use a modulator that can modulate the femtosecond laser pulses according to the incoming data stream (e.g., using on-off keying). The encoded pulses are propagated over a 2.5-km fiber link which uses dispersion compensating fiber (DCF) to compensate both the second and most of the third-order dispersion of the standard telecom fiber. Dispersion compensation is crucial since the encoding–decoding operation requires linear and substantially dispersion free pulse propagation. The transmission distance in femtosecond optical CDMA is limited mainly by the effectiveness of the dispersion management scheme used. Although we currently demonstrate propagation over only 2.5 km, by using programmable third-order dispersion correction in the encoder we have achieved almost dispersion free transmission for sub 500 fs pulses. This opens the possibility of having longer propagation distances of tens of kilometers. In this paper we give a comprehensive description of our femtosecond CDMA experiments, both at the subsystem and system level, including new results on encoding–decoding of femtosecond pulses after propagation through fiber, programmable dispersion compensation of coded-pulses, system results after higher order dispersion compensation, and system results for encoding–decoding with codes of different lengths.

In the following, Section II describes the different individual component technologies used to construct the CDMA test bed and presents subsystem level results. Section III presents system level results with all the CDMA subsystems connected together. In Section IV, we discuss some limitations of our ultrashort pulse CDMA implementation as revealed by the experiments. In Section V we conclude.

II. CDMA Component Technologies

The CDMA link integrates together several novel subsystems including femtosecond lasers and amplifiers, femtosecond fiber pig-tailed pulse shapers for encoding and decoding, femtosecond dispersion compensation and ultrafast nonlinear thresholders. This section describes the various building blocks and presents subsystem level experimental results.

A. Femtosecond Lasers and Amplifiers

Ultrashort optical CDMA requires femtosecond laser pulses as they provide the wide bandwidth and phase coherence necessary for the encoding–decoding operation. The lower limit on the shortest femtosecond pulse that can be used is placed by the effectiveness of the dispersion compensation scheme over the transmission distance. The upper limit on the longest pulse that can be used is placed by the minimum bandwidth required to code the ultrashort pulses, and the short pulsewidth required for effective high contrast thresholding. Due to these conflicting requirements for optimal operation of the different subsystems that make up the CDMA system, a pulsewidth of a few hundred femtoseconds was chosen for our experiments. Although several different techniques for femtosecond pulse generation in the 1.55 μm communication band exist, a passively mode-locked fiber laser was used due to its advantages of ease of construction and compatibility with all-fiber systems. Our femtosecond laser source is a passively mode-locked stretched-pulse all-fiber ring laser [21] that generates $\sim$62 fs pulses with a bandwidth of $\sim$60 nm. The laser output is externally filtered by a bandpass filter resulting in $\sim$275 fs pulses, with an average power of $\sim$40 μW, at a repetition rate of $\sim$30 MHz. A complete description of the laser construction may be found in [33]; only the intensity autocorrelation traces and spectra from the laser before and after the bandpass filter are shown in Fig. 2 demonstrating clean transform-limited laser operation. Note that although our 30 MHz pulse source was sufficient for characterizing the fidelity of the different CDMA operations, higher repetition rate sources would be required in a practical system.

Two amplifiers are used in the ultrashort pulse optical CDMA link. First, a preamplifier directly after the filtered laser

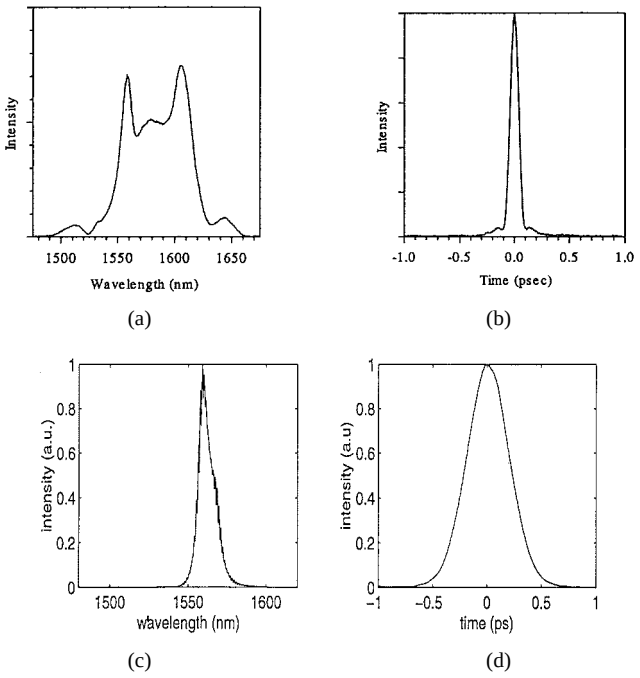

Fig. 2. Autocorrelation data and power spectra at the output of the femtosecond laser before and after bandpass filtering. (a) spectrum before filtering, (b) autocorrelation (∼62 fs intensity FWHM) before filtering, (c) spectrum after filtering, and (d) autocorrelation (∼275 fs intensity FWHM) after filtering.

source to compensate for the insertion loss of the encoder and the link, and second a postamplifier after the decoder to ensure adequate power for nonlinear thresholder operation. Although the two amplifiers were designed to provide different levels of amplification and output saturation powers, their general construction is quite similar. Fig. 3 shows a schematic of the preamplifier. Chirped pulse amplification technique [22], [23] is used to reduce the nonlinear effects in the amplifier. Input pulses from the laser are first stretched by passing them through ∼60 m of single mode fiber. They are then amplified by about ∼15 dB by passing through ∼18 m of erbium fiber which serves as the gain medium. The erbium fiber is pumped by 980 nm light from a Ti-Sapphire laser coupled to the amplifier through a WDM coupler. Monitors for both the pump and input signal are provided to measure input signal and pump power levels. Isolators at the input and output are used to reduce any feedback effects that can reduce the gain and output power. The preamplifier was designed to generate ∼1.2 mW of power at 1550 nm when pumped by ∼24 mW of pump power. The amplified pulse is compressed by using a dispersion-compensating fiber that compresses the pulse to its transform limited value. The amplifier produces ∼375 fs pulses, the pulse being broadened due to gain narrowing effects in the erbium fiber. The output pulses are taken from the 90% port of a 10–90% output coupler. The postamplifier follows the same construction as the preamplifier, with the longer length (∼25 m) of erbium fiber to give higher output powers. The postamplifier is designed to deliver up to ∼20 mW of output power when pumped by ∼130 mW of pump power. At higher output power levels, in addition to gain narrowing in the amplifier, we see some nonlinear effects in

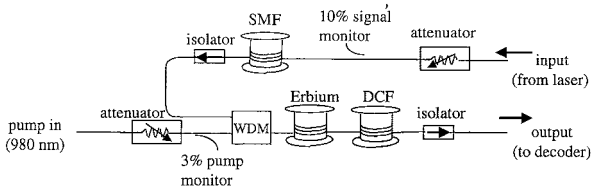

Fig. 3. Chirped pulse amplification erbium doped fiber amplifier.

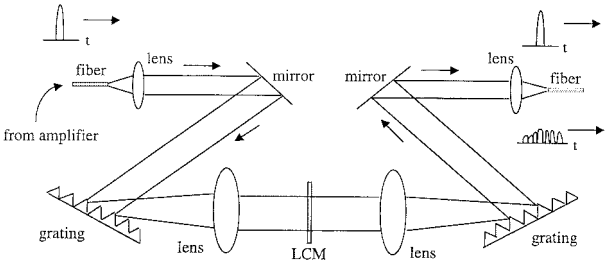

Fig. 4. Fiber-pigtailed programmable liquid crystal modulator pulse shaper.

the compressed pulses and the pulses are further broadened to between ∼600–900 fs.

B. Femtosecond Fiber Pig-Tailed Pulse Shapers for Encoding and Decoding

The femtosecond optical CDMA scheme is based on encoding and subsequent decoding of ultrashort light pulses. We accomplish this encoding–decoding operation by using femtosecond pulse-shapers [24]–[27] which offer high-resolution pulse shaping, programmability and the flexibility to apply arbitrary phase codes of different code lengths. Encoding and decoding of femtosecond pulses was previously demonstrated at a visible wavelength [24], [25], but in that arrangement, the encoding–decoding operation was performed by using two fixed conjugate phase masks placed successively in the same pulse-shaper. We demonstrate here programmable encoding–decoding operation at 1.55 μm communications wavelength in two separate pulse-shapers, and also demonstrate encoding–decoding when the two pulse-shapers are separated by a 2.5-km fiber link. We have also fiber-pigtailed our pulse shapers, which increases the ease with which we can either connect the pulse-shapers in the whole system, or disconnect them for individual measurements. Fiber-pigtailing also has the advantage that the pulse-shapers have to be aligned only once during the initial construction phase. We have achieved a low fiber-to-fiber insertion loss of only 5.3 dB. To our knowledge, these are the first experiments demonstrating femtosecond pulse-shaping operation at 1.55 microns using fiber-pigtailed pulse-shapers, and also the first demonstration of femtosecond encoding–decoding operation using such pulse-shapers.

The experimental arrangement of the pulse-shaper is shown in Fig. 4. In the pulse-shaper, collimated light from the input fiber pigtail is first diffracted off a grating (1100 lines/mm) and the different spectral components are then collected and focused by an achromatic lens (focal length = 190 mm). The incident angle and diffraction angles are approximately 43 and 75°, respectively. At the focal plane of the lens, the spectral components of the input pulse are linearly spatially separated.

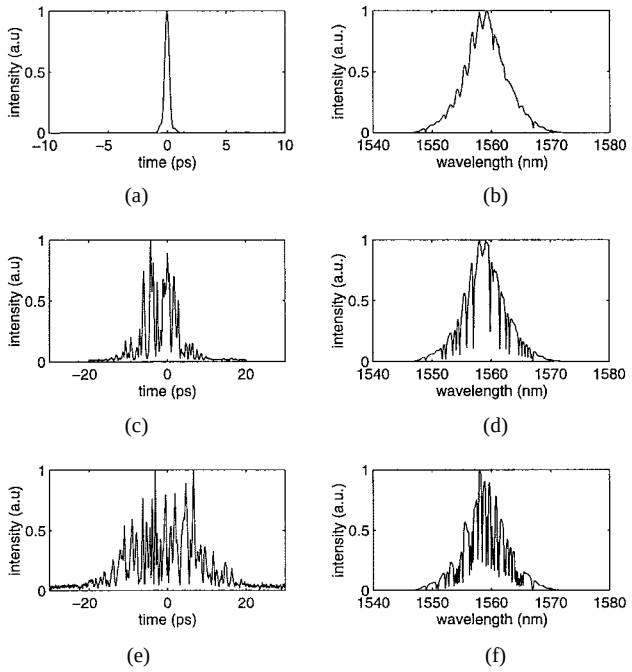

Fig. 5. Cross-correlation data and power spectra at the output of a single pulse shaper. (a) Output pulse (∼440 fs) with constant phase applied to the pulse shaper, (b) output pulse with 31 element M-sequence coding, (c) output pulse with 63 element M-sequence coding, and (d)–(f) power spectra corresponding to (a)–(c), respectively.

The liquid crystal modulator (LCM; CRI model SLM-128) is used to set the spectral phases to a length 31or length 63 M-sequence (MS) pseudorandom phase-code (which encodes the pulses into 10–20 ps wide pseudonoise bursts) or held constant leading to essentially unchanged uncoded pulses. The LCM has a fully programmable linear array of 128 pixels with 100 μm center-to-center pixel spacing, and individual pixels can be controlled by applying up to 4096 different drive levels resulting in phase shifts from 0–4π [26]. A length 31 MS, for example, consists of a pattern of "1"'s and "0"'s 31 bits in length that is accommodated by the 128 pixels of the LCM by assigning four pixels to each bit. For MS bits equal to one, the phases of the corresponding LCM pixels are set to π radians; for bits equal to zero, the phase is set to 0 radians. The rest of the pulse-shaper consists of a second matched achromatic lens and grating which reassembles the different spectral components into a single collimated output beam which is then coupled back into an output fiber pigtail. Note that two half waveplates were used, before and after the LCM, respectively, since the polarization state for operation of the LCM was orthogonal to that required by the gratings for optimum diffraction efficiency.

Fig. 5 shows measurements of time-domain output waveforms and spectra where the LCM is programmed for either a constant phase (no encoding) or length 31 or 63 M-sequence phase codes. The time-domain measurements are intensity cross-correlation data using unshaped pulses from the laser as a reference; to a good approximation they represent the actual output temporal intensity profiles. The holes in the spectrum seen in Fig. 5(e) and (f) are related to diffraction effects arising from the frequency components of the input pulse which fall at 0–π transitions of the LCM's in the pulse shaper [22], [27]. Each individual frequency component of the input pulse has a finite spatial extent at the mask plane (as determined by the input beam diameter), which may cause the different spatial regions of one particular frequency component to see different phase retardations. The output fiber pigtail acts as a spatial filter that samples the frequency dependent diffraction pattern from the LCM. This results in phase to amplitude conversion that leads to the observed dips in the spectrum. These effects are more pronounced for the length 63 MS due to a larger number of 0–π transitions.

We can model these diffraction effects using a simple theoretical analysis published previously [27], [28]. The response of the pulse shaper can be characterized in the frequency domain by

$$E_{\rm out}(\omega) = E_{\rm in}(\omega)H(\omega) \tag{1}$$

where $E_{\rm in}(\omega)$ and $E_{\rm out}(\omega)$ are the Fourier transforms of the input and output electric fields, respectively, and $H(\omega)$ is the complex frequency response of the linear filter acting on the femtosecond pulses. $H(\omega)$ can be related to the actual physical masking pattern with complex transmittance $M(x)$ (i.e., the spatial phase pattern on the LCM) by

$$H(\omega) = \left(\frac{2}{\pi w_0^2}\right)^{1/2} \int dx\, M(x)\, e^{-2(x-\alpha\omega)^2/w_o^2}. \tag{2}$$

Here α is the spatial dispersion of the pulse shaper with units cm (rad/s)$^{-1}$ and w_o is the radius of the focused electric field beam profile at the masking plane (for any single frequency component). Expressions for α and w_o in terms of the pulse shaper parameters and input beam profile are given in [27]. Assuming that the Gaussian mode selected by the output fiber is matched to the mode from the input fiber, as is the case in our experiments, (2) completely accounts for diffraction effects arising in the pulse shaping process. Equation (2) shows that the effective filter in the frequency domain is the mask function $M(x)$ convolved with the *intensity* profile of the beam. The main effect of this convolution is to limit the full-width at half-maximum (FWHM) spectral resolution $\delta\omega$ of the pulse shaper to $\delta\omega \cong (\ln\ 2)^{1/2} w_o/\alpha$. Physical features on the mask smaller than $\sim w_o$ are smeared out by the convolution, and this limits the finest features which can be transferred onto the filtered spectrum. One consequence of this picture is that wavelength components impinging on mask features which vary too fast for the available spectral resolution are in part diffracted out of the main beam and hence not coupled into the output fiber. This leads to the phase-to-amplitude conversion evident in Fig. 5. Improved spectral resolution can be achieved, e.g., by increasing the input beam size to decrease w_o.

Fig. 6 shows a comparison of the experimental power spectrum for coding with a length 31 MS with a simulation based on (1) and (2). The simulation parameters (α and w_o) were found by matching the locations and widths of dips in experimental and simulated power spectrum for a very simple setting of the LCM where pixels 20, 64, and 110 were set for π phase shift, with all other pixels set for zero phase shift. This resulted in $\alpha \cong 9.6 \times 10^{-14}$ cm (rad/s)$^{-1}$ (0.75 mm/nm) and $w_o \cong 120$ μm. Using these same parameters, excellent

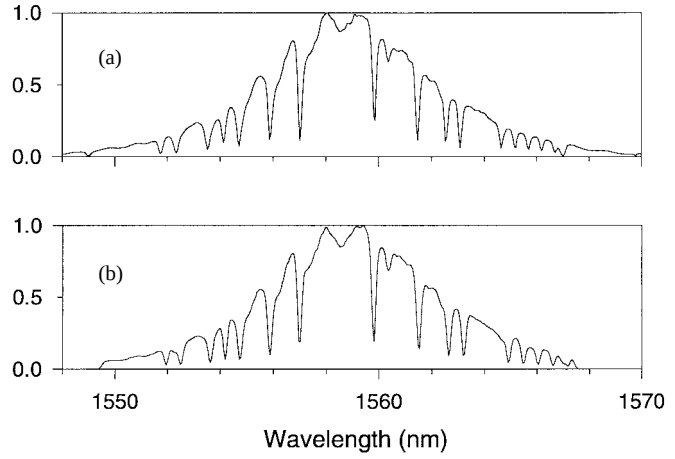

Fig. 6. Experimental (a) and simulated (b) power spectra for coding with a length-31 M-sequence spectral phase code using a single phase shaper.

agreement between the actual and simulated spectra for length-31 MS coding is obtained, as seen in Fig. 6. Similar agreement is obtained for coding with M-sequences of other lengths and for encoding–decoding experiments (discussed next), in all cases using the same values for α and w_o.

Encoding and decoding experiments are performed by taking pulses exiting from the first pulse-shaper (encoder) and inputting them through a fiber pigtail into an identically constructed second pulse-shaper (decoder). The encoder and decoder are matched to within a pixel accuracy of the LCM's, as measured by a 0.08 nm resolution optical spectrum analyzer. Note that due to aberrations in the pulse shaper arising due to the very large diffraction angles, as well as the interactions of polarization mode dispersion effects in the fiber components with polarization sensitive devices (e.g., gratings) in the pulse shaper, the overall output pulse after two pulse shapers is broadened to ∼500 fs. Fig. 7 shows experimental cross-correlation data and corresponding output spectra for the encoding–decoding operation for length 31 MS phase codes. Fig. 7(a) shows normalized intensity cross-correlation data for an uncoded pulse where a constant phase is applied to the LCM's in both the encoder and the decoder. Fig. 7(b) shows cross-correlation data for a properly decoded pulse (PDP) for 31 element MS encoding–decoding when the phase codes of the two LCM's match, and Fig. 7(c) shows an improperly decoded pulse (IPDP) when the phase codes on the two LCM's do not match. Note that the vertical axes in Fig. 7(b) and 7(c) are normalized to the peak intensity of Fig. 7(a). Fig. 7(d)–(f) show the output spectra corresponding to Fig. 7(a)–(c) respectively. It can be seen from Fig. 7(a) and (b) that although the encoding–decoding process restores the pulse-width of the PDP to its original uncoded value, its peak intensity is reduced to ∼60% of that in Fig. 7(a). As before, diffraction effects inherent in the pulse-shaping process cause a decrease in the peak intensity and the appearance of a pedestal in the decoded pulse. They are also responsible for the holes seen in the spectra of Fig. 7(e) and (f). Note that the spectrum of the IPDP shows more holes. This is because the MS in the encoder and decoder do not match resulting in a larger number of 0–π

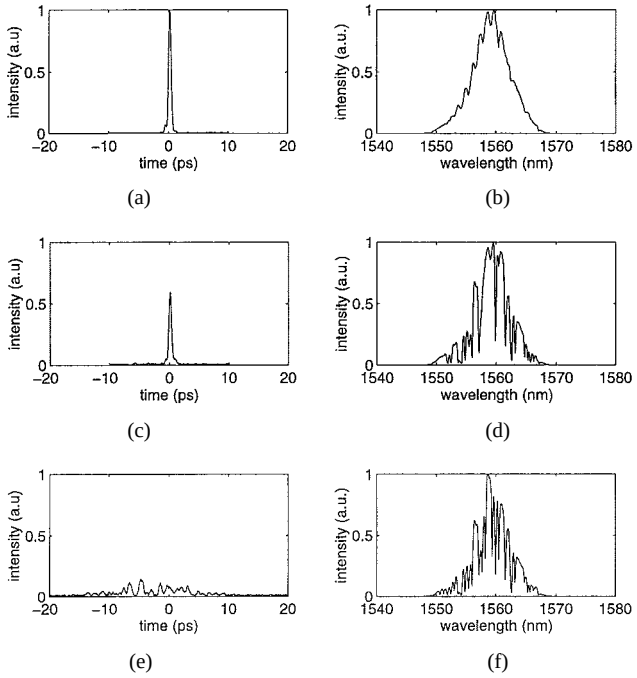

Fig. 7. Cross-correlation data and power spectra after encoding–decoding with two pulse shapers for 31 element M-sequence coding. (a) Output pulse (∼500 fs) with constant phase applied to both pulse shapers, (b) properly decoded output pulse (∼510 fs), (c) improperly decoded output pulse, and (d)–(f) power spectra corresponding to (a)–(c), respectively.

transitions. Note also that the holes observed in the spectrum of the PDP [Fig. 7(e)] are wider than those observed in the spectrum of the encoded pulse [see Fig. 5(e)]. This occurs due to phase to amplitude conversion at the same pixel position (and therefore at the same wavelength) arising independently in both the encoder and decoder. Similar trends were observed for length 15, 63, and 127 M-sequences. In all cases, the decoded pulse exhibited a main peak duration comparable to that of the uncoded case and intensity substantially above a lower intensity pedestal. However, the holes in the spectrum, the drop in peak intensity, and the overall energy loss in the decoding process became more severe for longer code lengths. Table I shows the peak intensity and the energy of the PDP, normalized to the case of constant spectral phase in the encoder and decoder, for length 15, 31, and 63 codes. The experimental results are in excellent agreement with simulations, using the same values for α and w_o as previously. The comparison shown in Table I is perhaps the most demanding test of (2) to date, in terms of the complexity of the experimental waveforms. The excellent results suggest that this simulation procedure can be used to predict coding-decoding performance for a broad range of experimental parameters. Based on the data in Table I, we have selected length 31 and 63 MS codes for our system studies, although longer codes (e.g., 127) would be desirable if sufficient spectral resolution were available.

C. Femtosecond Dispersion Compensation

Transmission of femtosecond pulses over kilometer distances requires the simultaneous compensation of both the quadratic dispersion and most of cubic dispersion of the input pulse. In femtosecond optical CDMA dispersion

TABLE I
NORMALIZED PEAK POWER AND ENERGY OF PROPERLY DECODED PULSES FOR CODING WITH LENGTH 15, 31, AND 63 M-SEQUENCES. THE POWER AND ENERGY ARE NORMALIZED TO THE POWER AND ENERGY OF PULSES PASSING THROUGH AN ENCODER AND DECODER PAIR EACH SET FOR CONSTANT SPECTRAL PHASE

M-sequence length	Normalized peak power		Normalized energy	
	Experiment	Theory	Experiment	Theory
15	73.2%	74.1%	83.1%	78.8%
31	59.0%	65.5%	74.6%	75.0%
63	28.5%	35.7%	46.4%	48.8%

compensation is necessary for two reasons. First, since the CDMA scheme needs linear pulse transmission due to the phase sensitive encoding–decoding operation, we cannot use soliton propagation. Second, uncompensated dispersion will severely degrade the contrast between properly and improperly decoded pulses. Several dispersion compensation schemes applicable to femtosecond pulse transmission have been demonstrated before that can compensate the chromatic dispersion of standard single-mode fibers [29]–[33]. Our dispersion compensation scheme based on the use of dispersion compensating fiber (DCF) [34] to compensate the quadratic dispersion and most of the cubic dispersion of standard single mode fiber (SMF), has been detailed previously [31]–[33]. Such an SMF-DCF fiber link has much lower third-order dispersion than conventional dispersion shifted fiber. Further, by applying a cubic phase to the pixels of the programmable liquid crystal (LCM) in the encoder, we can almost completely remove the small residual third-order dispersion of the SMF-DCF link resulting in essentially distortionless transmission of sub-500 fs pulses over 2.5 km of optical fiber [33]. To our knowledge, these were the first experiments of dispersion compensation on a femtosecond time scale using dispersion compensating fiber [31] and the first demonstration of almost dispersion free transmission by applying residual phase correction via a programmable pulse-shaper [33]. In addition to its applicability in femtosecond CDMA systems, this dispersion compensation scheme can be used in any other transmission scheme that uses ultrashort pulses.

Fig. 8 shows intensity cross-correlation data for pulses at the input and output of the 2.5 km SMF-DCF link. The link is composed of ~2060 m of SMF and ~445 m of DCF fiber, dispersion optimized by adjusting the lengths of the individual fibers to give the shortest output pulse. Fig. 8(a) shows the input pulse and Fig. 8(b) shows data for the same pulse after the 2.5 km link. The output pulse is broadened to ~580 fs with some small oscillation in the tail indicating residual positive third-order dispersion. In contrast, we estimate that the pulse after propagating down the 2 km length of SMF only would broaden to ~200 ps. The residual dispersion is further compensated by applying an appropriate phase variation across the pixels of the LCM in the encoder, resulting in almost complete dispersion compensation as seen in Fig. 8(c). The phase pattern applied to the LCM [see Fig. 8 (d)] is discretely sampled over the entire 128 LCM pixels, but since the phase difference between the first and last pixel is quite small (~2.1π), the sampling can be considered almost continuous. This leads to the almost exact phase correction of the residual

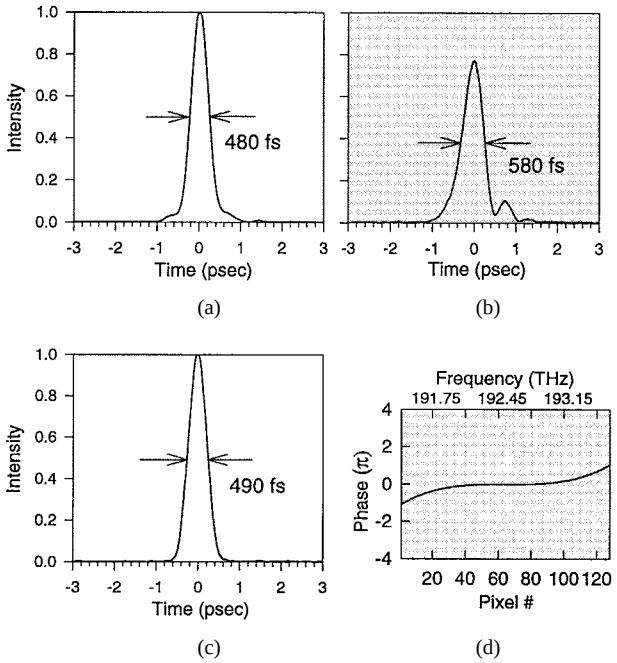

Fig. 8. Cross-correlation data for femtosecond dispersion compensation. (a) Input pulse to the 2.5 km link, (b) output pulse from the link when a constant phase is applied to the LCM, (c) output pulse with cubic phase correction applied to the LCM, and (d) the cubic phase correction function applied to the LCM pixels.

third-order dispersion in the link and thus to almost complete restoration of the output pulse.

The pulse shaper can also be programmed for simultaneous dispersion compensation and decoding (or encoding). This is accomplished by summing (modulo 2π) the phases needed for decoding and for dispersion compensation. Fig. 9 shows intensity autocorrelation data for properly and improperly decoded pulses using a length 63 MS code for the case of (a) only a few meters of fiber between encoder and decoder, and (b), (c) 2.5 km dispersion compensated link connecting encoder–decoder, either (b) without or (c) with one of the LCM's also used to trim out the residual phase from the fiber link. Note that in each case the amplitude of the PDP is normalized to unity, and a small coherence spike is observed at the origin for the IPDP as is expected in autocorrelation traces for pseudonoise bursts [35]. Compared to Fig. 9(a), we can see from Fig. 9(b) that residual dispersion in the fiber link has broadened the main peak and reduced the contrast between the PDP and IPDP autocorrelations. In this case the fiber link was adjusted so that small amounts of residual quadratic and cubic dispersion were both present. By programming an LCM for simultaneous decoding and dispersion compensation as in Fig. 9(c), the duration of the autocorrelation peak and contrast ratio between the PDP and IPDP is restored to that observed with only a few meters of fiber. The ability to perform decoding and programmable fine tuning of the dispersion compensation in the same module relaxes to some degree the precision with which the fixed dispersion compensator must be set.

D. Ultrafast Nonlinear Thresholders

Optical CDMA receivers need a thresholding device to distinguish between properly decoded femtosecond pulses and the

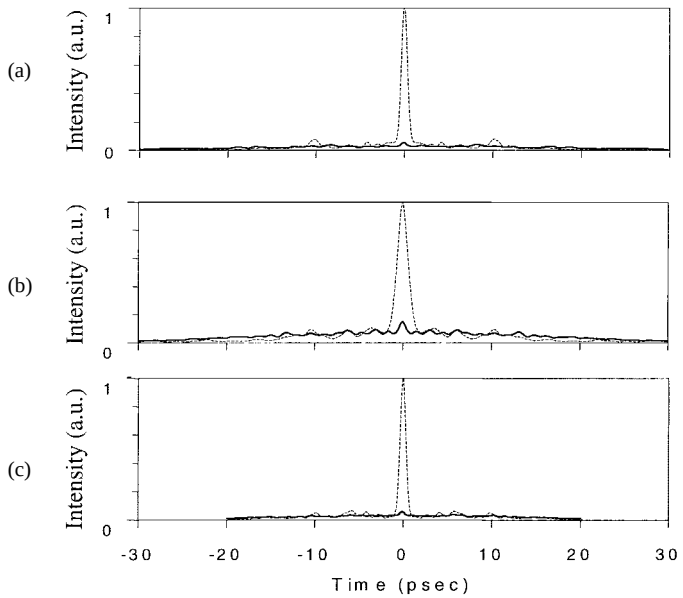

Fig. 9. Intensity autocorrelation data for spectral encoding and decoding separated by fiber, using length-63 M-sequences. Both properly (dashed line) and improperly (solid line) decoded pulses are shown. (a) Only fiber pigtails (a few meters) separate encoder and decoder. (b) 2.5 km dispersion-compensated links, without phase trimming by LCM. (c) 2.5 km dispersion-compensated link, with phase trimming by LCM.

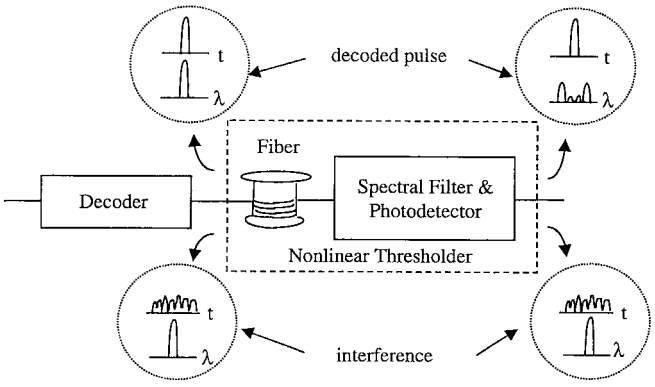

Fig. 10. Schematic of the nonlinear thresholder.

equally energetic improperly decoded picosecond interference signals. This required discrimination is achieved by exploiting nonlinear frequency shift effects in optical fibers. We use two nonlinear effects in optical fibers, namely, nonlinear self phase modulation [36]–[38] and nonlinear Raman effects manifested as the soliton self frequency shift [39], [40]. In both of these effects when a high intensity femtosecond pulse is propagated in an optical fiber, the output pulse exhibits frequency shifts (away from its mean input frequency), the exact nature of the shift depending on the particular nonlinear process. The lower peak power longer duration interference signals do not exhibit any significant changes to their frequency spectrum. Fig. 10 shows the block diagram of the nonlinear thresholder, which is combination of a suitable length of optical fiber followed by a long wavelength pass spectral filter. The long wavelength pass filter is one half of a pulse shaper, with the LCM replaced by a knife-edge mounted on a translation stage. This arrangement allows us to change the filter cutoff wavelength by simply moving the spatial position of the

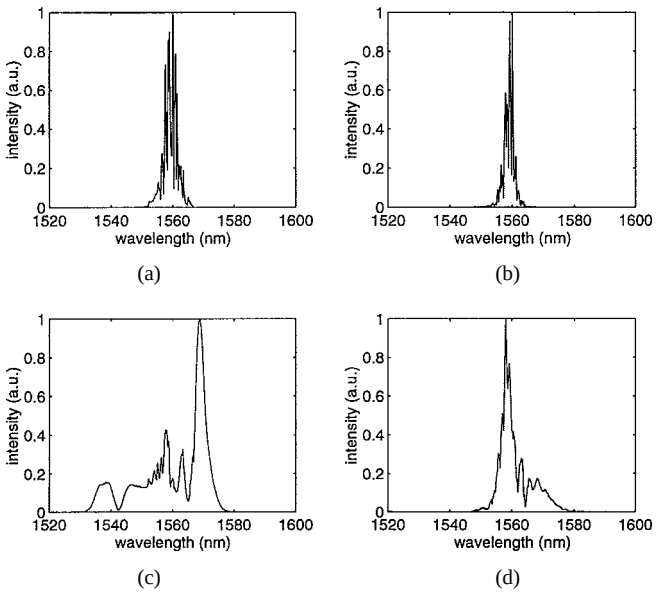

Fig. 11. Power spectra at the output of the nonlinear thresholder for two different thresholder fibers. (a) Output power spectrum for $\lambda_0 \sim 1559$ nm DSF thresholder fiber for coded pulses, (b) output power spectrum for $\lambda_0 \sim 1559$ nm DSF thresholder fiber for uncoded pulses, (c) output power spectrum for $\lambda_0 \sim 1547$ nm DSF thresholder fiber for coded pulses, and (d) output power spectrum for $\lambda_0 \sim 1547$ nm DSF thresholder fiber for uncoded pulses. For (a) and (b) the average power is 0.44 mW and for (c) and (d) the average power is 1.84 mW.

knife-edge. The spectrally filtered pulse exiting the filter is focused into a photodetector. The combination of spectral filter and photodetector converts any frequency shifts occurring in the thresholder fiber into amplitude variations which can be detected by the photodetector.

We earlier demonstrated two different thresholder designs for a stand-alone thresholder by propagating coded and uncoded pulse through the nonlinear fiber and obtained high contrast thresholding after the output filter [41], [42]. In the integrated system described later, such coded and uncoded pulses would correspond to improperly decoded and properly decoded pulses respectively. In the first design [41], both the uncoded femtosecond pulses and the coded interference signals were propagated through a dispersion shifted fiber (DSF) whose zero dispersion wavelength coincided with the center wavelength of the transmitter laser (∼1559 nm). Nonlinear self-phase modulation effects cause the spectrum of the femtosecond signal pulse to split and spread on either side of the zero dispersion point while the low intensity picosecond interference signal remains at its original spectral position. Fig. 11(a) and (b) show power spectra at the output of the thresholder fiber for coded and uncoded pulses respectively clearly revealing the differences between the two. The pulses were coded using a length 63 M-sequence. The long wavelength pass filter at the output transmits the shifted portion of the uncoded pulse and rejects the unshifted coded pulse. High contrast ratios of 30 dB were obtained using 500 m of fiber at average power levels of 0.44 mW for 1569 nm cutoff wavelength of the output spectral filter (see Fig. 12). Fig. 12 also shows the variation of the contrast ratio for the various cyclic shifts of the 63 element M-sequence (thus representing different codes or interfering users) for two

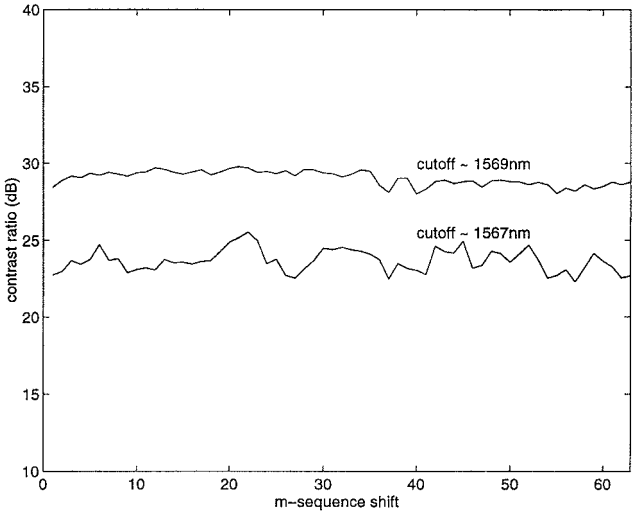

Fig. 12. Variations of the contrast ratio at the output of the nonlinear thresholder for two different positions of the long wavelength pass filter for coding using the cyclic shifts of a length 63 M-sequence. The thresholder fiber has $\lambda_0 \sim 1559$ nm and the average power in the fiber is 0.44 mW.

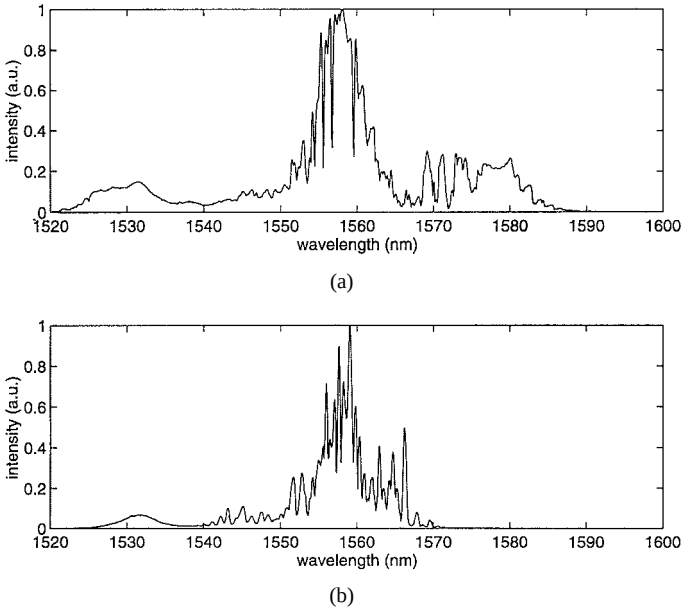

Fig. 13. Power spectra after the thresholder fiber for 31-element M-sequence encoding–decoding and propagation over a 2.5 km link. (a) Properly decoded pulse and (b) improperly decoded pulse. The thresholder fiber is the $\lambda_0 \sim 1559$ nm DSF and the average power is ~2.4 mW.

different cutoff wavelengths of the output spectral filter. The contrast ratio is seen to be only minimally affected by the particular choice of the M-sequence. The energy conversion efficiency (ratio of energy detected after the spectral filter to energy in thresholder fiber) for this thresholder was about 10%. The main advantage of this design is the lower average power required for obtaining high contrast ratios. The main disadvantage is the requirement to closely match the zero dispersion wavelength of the thresholder fiber to the center wavelength of the source laser.

In the second design [42], a DSF fiber with zero dispersion wavelength less than the center wavelength of the source laser ($\lambda_o \sim 1547$ nm) was used so that the optical spectrum lies entirely in the anomalous dispersion regime of the fiber. The nonlinear Raman effect and the resulting soliton-self-frequency shift cause the mean wavelength of the high intensity properly decoded signal to shift to longer wavelengths, while the low intensity interference signal remains at its original spectral position. Fig. 11(c) and (d) show power spectra at the output of the thresholder fiber for coded and uncoded pulses respectively for this design. Again, a properly positioned long wavelength pass filter can transmit the shifted signal and reject the interference signal giving high contrast thresholding. A nonlinear thresholder having 36 dB contrast ratio for 1.84 mW average power in the thresholder fiber was demonstrated using 340 m of this dispersion shifted fiber for 1577 nm cutoff wavelength of the output spectral filter. The main advantage of this design is the flexibility of choosing the zero-dispersion wavelength, although it is achieved at the expense of higher average powers required for high contrast thresholding. To our knowledge, these were the first experiments demonstrating nonlinear thresholding operation in optical fibers with high contrast ratios.

III. System Results

We have so far discussed the various CDMA subsystems and presented experimental data for their performance. We now discuss system level results for a single transmitter-single receiver experiment including encoding, fiber propagation, decoding, and thresholding. For single user operation, the following three parameters will chiefly determine the system performance. First, the fidelity of the encoding–decoding operation with the 2.5-km fiber link in-between the encoder and decoder. Second, the effectiveness of the dispersion compensation scheme for coded pulse propagation with and without residual third-order dispersion correction, and finally, the contrast ratio after the nonlinear thresholder between a properly and improperly decoded pulse.

Fig. 13 shows power spectral data at the output of the thresholder for PDP and IPDP for 31 element M-sequence (MS) phase coding. In the system experiments, the thresholder fiber with zero dispersion wavelength at 1559 nm was used, primarily because it requires lower average powers to give high contrast thresholding. By comparing Fig. 13(a) and (b) we note that the spectrum of the PDP has split to either side of the zero dispersion point. The peak at 1530 nm observed on both the spectra is due to the amplified spontaneous emission from the erbium doped fiber amplifier in the receiver. Fig. 14 shows the encoding–decoding autocorrelation data after the decoder and the corresponding power spectral data after the thresholder for 63 element MS encoding–decoding, clearly demonstrating CDMA operation for longer code lengths. The contrast ratios (defined as the ratio of the energy of the PDP to that of the IPDP) after spectral filtering in the nonlinear thresholder are plotted Fig. 15 for length 31 and length 63 MS phase coding. The cutoff wavelength of the spectral filter is ~1573 nm. The horizontal axis in the figure is the pump power applied to the EDFA in the receiver, and the corresponding variation of the average signal power in the thresholder fiber would be from ~1 to 2.5 mW. As seen in the

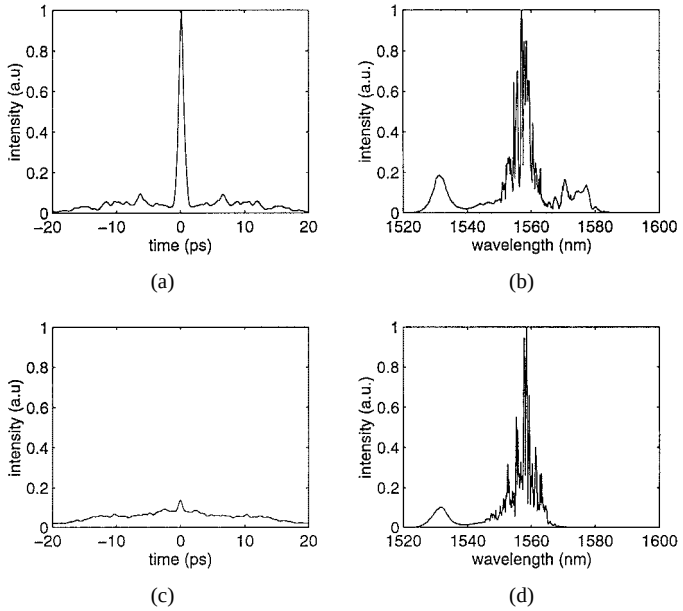

Fig. 14. Autocorrelation data after the decoder and power spectra after the thresholder for 63 element M-sequence encoding–decoding. (a) Autocorrelation of properly decoded pulse, (b) autocorrelation of improperly decoded pulse, (c)–(d) power spectra after the thresholder corresponding to (a)–(b), respectively. The average power in the thresholder fiber is ∼2.3 mW.

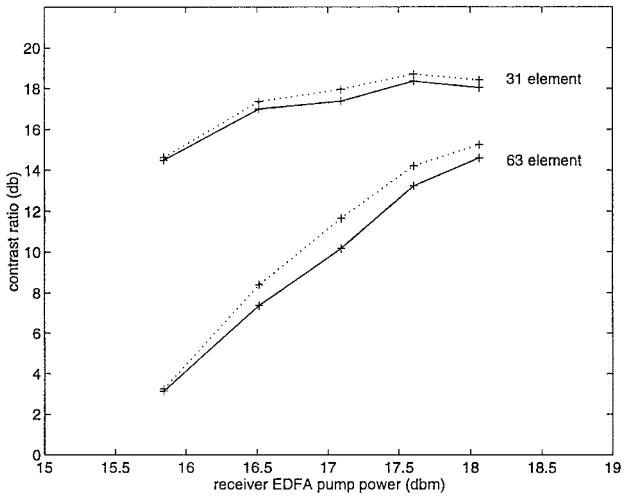

Fig. 15. Contrast ratios at the output of the CDMA test bed for 31 element and 63 element M-sequence encoding–decoding. Solid lines correspond to no cubic phase correction in the encoder LCM and dotted lines correspond to cubic phase correction in the encoder LCM. The cutoff wavelength of the spectral filter in the nonlinear thresholder is 1573 nm in each case.

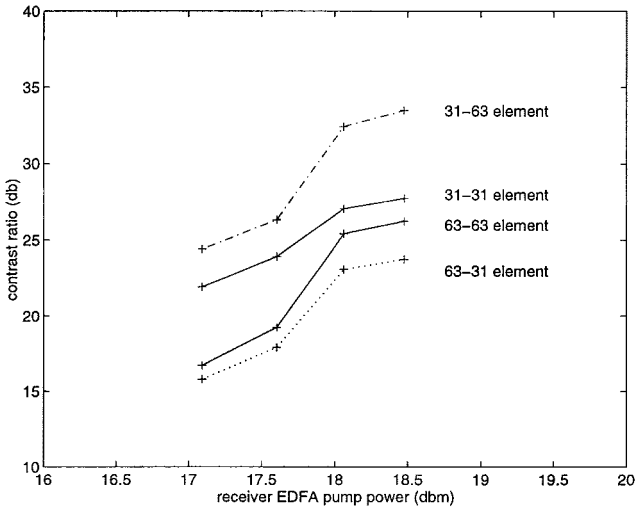

Fig. 16. Contrast ratios at the output of the CDMA test bed for 31 element and 63 element M-sequence encoding–decoding for (>1573 nm) cutoff wavelength of the nonlinear thresholder (both shown by solid lines). The dashed-dot line is for a 31-element M-sequence user when the interfering user has a 63-element M-sequence phase code. The dotted line is for a 63-element M-sequence user when the interfering user has a 31-element M-sequence phase code.

figure, a slight increase in the contrast ratio is observed when the LCM provides third-order dispersion correction. Note that the contrast ratio for 31 element MS encoding–decoding is larger than that for 63 element MS encoding–decoding, and the difference between the two is more prominent at lower pump powers. This is because the PDP has a larger peak power (and also larger average power) for 31 element MS coding than for 63 element MS coding (see Table I). At lower pump powers the EDFA gain is fairly constant, resulting in the amplified properly decoded pulse for 31-element coding having a larger peak power, and therefore higher frequency shifts, and higher contrast ratios. At higher pump powers, gain saturation effects come into play and the differences in the contrast ratios are smaller. The contrast ratio in both cases is limited by the long wavelength ASE components of the EDFA in the receiver. Compared to the earlier thresholding experiments using only a single pulse shaper for encoding (and only a single amplifer), ASE is a more serious issue in the integrated system, since two EDFA's are employed. Note also that for 31 element MS coding, the contrast ratio curve is quite flat over the entire range of average powers in the thresholder fiber indicating that the contrast ratio is not very sensitive to the exact value of the average power. This is important as it gives some design margin for constructing the receiver amplifier especially under multiple user operation.

To get around the ASE limitation, we have two choices. First, we can install a bandpass filter after the receiver EDFA that eliminates the long wavelength ASE components. Second, we can engineer the spectral filter in the thresholder and set its cutoff wavelength to a much longer wavelength (>1573 nm) effectively blocking out as much long wavelength ASE as possible. Note that in the second approach we also reduce some of the signal from the properly decoded pulse. This is however not a serious limitation as long as we have sufficient signal for detection, and the reduction of the long wavelength ASE is greater than the reduction in the properly decoded signal. Using the second approach we increased the contrast ratio of the CDMA test bed to 27.5 and 25 dB for 31 element and 63 element M-sequence coding respectively (compared with ∼18 and ∼15 dB in Fig. 15) as shown by the solid lines in Fig. 16. Note again that the horizontal axis in the figure is the pump power applied to the EDFA in the receiver, and the corresponding variation of the average signal power in the thresholder fiber would be from ∼1.5 to 2.75 mW.

We also tested one more variation of the code length dependence of the contrast ratio, namely when the interfering

user has encoded its data using a different length code-sequence than the intended user. We can now have some users who encode their data with length 31 MS transmitting information over the same optical channel with other users who encode their data with length 63 MS. Note that in optical CDMA the intended receiver has to be provided with a-priori information about the exact nature of the code sequence of the transmitter. Hence having different users encoding their data bits with different length MS does not add any more complexity to the system. When the CDMA receiver decodes an incoming interference signal, its output remains as a low intensity pseudonoise burst irrespective of the exact nature of the code length of the interfering user. This can be observed from Fig. 16, where it should be noted that the contrast ratio has actually increased for length 31 MS coding when the interfering user has its bits coded with a length 63 MS. This can be attributed to a combination of two factors. First, an interfering user with 63 element MS coding has a longer temporal spread of its encoded pulse [also compare Fig. 5(b) and (c)] than an interfering user with 31 element MS coding. Hence after decoding, a length 31 MS-length 63 MS improper decoding results in a longer duration improperly decoded pulse than a length 31 MS-length 31 MS improper decoding. Since the thresholder is a nonlinear device, a longer duration improperly decoded pseudonoise signal has relatively less spectral shifts than a shorter duration improperly decoded pseudonoise signal. (Note that the absolute spectral shifts in either case are much less than that for a properly decoded pulse). This explains the increase in contrast ratio. The second factor for this increase is the slightly higher loss in the decoder pulse shaper for 63 element MS coding than for 31 element MS coding. This would cause the decoder output to have different average powers depending on the specifics of the encoding–decoding process. The contribution due to this effect is expected to be small as measurements at the EDFA output for the two cases (i.e., length 31 MS-length 31 MS and length 31 MS-length 63 MS improper decoding) have shown only 5% difference in average powers. The contrast ratio for 63 element MS encoding–decoding is likewise higher than that for 63 element coding-31 element decoding. This also appears to be related to the temporal and intensity characteristics of the improperly decoded pulses. Note that for a given MS, translating the bit pattern by one-bit results in a new MS that is orthogonal to every other MS obtained by such bit translations. Hence, a length 63 MS can accommodate 63 possible users. A combination of length 63 and length 31 MS thus increases the number of addresses that can be assigned to users, and also shows the robustness of the optimal CDMA system when the interfering users have different types of codes.

IV. Discussion

Although the component technologies and the single-user system results in principle show potential for true multi-user operation, several factors may affect the practical implementation of the CDMA system in a multi-user environment. Some of the issues which would affect practical femtosecond CDMA operation are discussed in the following, with reference where applicable to our experimental results.

1) The current single user experiments running at pulse rates of ∼30 MHz required on the order of 1 mW for high contrast operation of the fiber nonlinear thresholder. In multi-user networking each receiver will see a sample of each of the multiple-access signals; therefore, the required postamplifier saturation power scales with number of users (as well as bit rate). For 30 users with ON–OFF keying at 1 Gb/s per user, each postamplifier will need to amplify to ∼500 mW. Although this is possible, for most applications such an amplifier will be too costly for use on a per node basis. Therefore, thresholding devices that can operate at lower power levels than in the current experiments are required. It may be possible to achieve some power reduction by using longer thresholder fibers or longer pulsewidths. Other technologies based on nonlinearities in guided wave optoelectronic devices may also offer some potential for lower operating powers [43], [44].
2) We have demonstrated distortionless transmission of sub-500 fs pulses over a 2.5 km dispersion compensated fiber link. Although programmable dispersion compensation in the encoder or decoder allows fine tuning of the overall dispersion balance, nevertheless each fiber link in the CDMA system will still need rather precise setting of its large fixed dispersion compensator. Greater precision will be needed if shorter pulses or longer fibers are desired, and this may ultimately limit the usable pulse width or fiber span.
3) Assuming adequate power budgets are available, the overall capacity in this ultrashort pulse CDMA scheme scales inversely with pulse width (for fixed code length) and increases strongly with increased code length (for fixed pulse width) [7]. Here we have demonstrated operation with 500-fs pulses and code lengths of 31 and 63. However, to obtain capacities in the range of tens of Gb/s to ∼100 Gb/s or above, one needs code lengths in the range from 127 to 511 and shorter pulse widths (∼100–300 fs). For the current pulse width longer code lengths (at least up to 127) should be possible by improving the pulse shaper spectral resolution. Shorter pulse widths would allow a greater increase in code length, since more spectrum is available for coding. To maintain shorter pulse widths, gain narrowing in the amplifiers, which is a significant limitation in the current experiments, must be avoided. Additionally, substantially longer code lengths would require LCM's (or other modulator array technologies) with more than the current 128 pixels.
4) The accumulated nonlinearity in the transmission fibers must remain small in order to avoid degrading the decoded pulses. On the other hand, if the transmitted power is too low, the power requirements of the nonlinear thresholder will place additional demands on the receiver amplifier. We have performed simulations and experiments showing that uncoded pulses can be transmitted with average powers up to the ∼1 mW

level in the current setup (at the same pulse repetition rate) before nonlinearities become evident [45]. Coded pulses (as here) have lower peak intensities and therefore are less susceptible to nonlinearities. Based on these considerations, at present we do not expect nonlinearities in the transmission channel to be a serious limitation. However, further study is needed to fully assess nonlinearity limits for femtosecond pulse transmission in dispersion compensated links with large pulse stretching and compression ratios.

5) In a N user system, the broadcast star architecture will lead to a factor of N splitting loss not present in the current single user experiments. This loss would have to be offset either by using a more powerful source (compared to the 40 μW after spectral filtering currently) or through additional amplification.
6) Even though we have demonstrated relatively low-loss filter pigtailed operation, the encoding–decoding device in its present form requires the use of bulk gratings and lenses which limits its use in practical applications. In the future this part of the system will have to be miniaturized, perhaps taking advantage of integrated wavelength division multiplexing technologies. Experiments demonstrating simple pulse shaping operation have been reported both using integrated acoustooptic tunable filters [46] and arrayed waveguide gratings [47], and a miniaturized and packaged pulse shaping setup used for gain equaliztion of amplified WDM systems was demonstrated in [48].

V. Conclusion

We have presented a detailed description of a femtosecond optical CDMA scheme. On the subsystem level, three main component technologies, namely, femtosecond encoding–decoding, femtosecond dispersion compensation, and ultrafast nonlinear thresholding, have been developed and characterized. The high fidelity femtosecond encoding–decoding obtained for length 63 and length 31 M-sequences has shown the potential for true multi-user operation. Femtosecond dispersion compensation, especially with residual third-order dispersion correction, should extend the propagation distance to over 10 km. The high-contrast thresholding should allow good discrimination against multi-access interference, although lower operating power would be desirable. On a system level, the ability to propagate a coded pulse and decode it with a 27.5 dB contrast against interference has the potential to extend optical CDMA beyond the single-user operation demonstrated here. Similarly, the high contrast ratios obtained for different length M-sequence coding makes it possible to add more addresses than would be available with a fixed single-length M-sequences. In conclusion, we have demonstrated for the first time the ability to propagate femtosecond optical pulses from CDMA transmitters to receivers in an integrated system including all the required operations needed for femtosecond pulse CDMA. In the future we plan to use this system as a test bed to investigate CDMA system performance during multiuser operation.

Acknowledgment

The authors would like to gratefully acknowledge A. Vengsarkar of Lucent Technologies, NJ, for providing the dispersion compensating fiber, V. DaSilva and M. Newhouse of Corning Inc., Corning, NY, for providing dispersion shifted and erbium doped fibers, and I. Duling of Naval Research Laboratory, Washington, DC, for helpful discussions related to erbium amplifiers. They would also like to thank A. Emmanuel and S. Shen for calibrating the LCM's, and D. Leaird for technical assistance.

References

[1] H. Onaka *et al.*, "1.1 Tb/s WDM transmission over 150 km 1.3 μm zero-dispersion single-mode fiber," in *Proc. Conf. Optic. Fiber Commun. (OFC'96)*, postdeadline paper pd19, San Jose, CA, 1996.
[2] A. H. Gnauck *et al.*, "One terabit/s transmission experiment," in *Conf. Optic. Fiber Commun. (OFC'96)*, postdeadline paper pd20, San Jose, CA, 1996.
[3] T. Morioka *et al.*, "100 Gb/s $\times$ 10 channel OTDM/WDM transmission using a single supercontinuum source," in *Proc. Conf. Optic. Fiber Commun. (OFC'96)*, postdeadline paper pd21, San Jose, CA, 1996.
[4] N. S. Bergano *et al.*, "100 Gb/s error free transmission over 9100 km using twenty 5 Gb/s WDM data channels," in *Proc. Conf. Optic. Fiber Commun. (OFC'96)*, postdeadline paper pd23, San Jose, CA, 1996.
[5] T. Naito *et al.*, "128-Gbit/s WDM transmission of 24 5.3-Gbit/s RZ signals over 7828 km using gain equalization to compensate for asymmetry of EDFA gain characteristics," in *Tech. Dig., Conf. Optic. Fiber. Commun. (OFC' 97)*, paper TuJ2, pp. 45–46, 1997.
[6] S. Kawanishi *et. al.*, "400 Gbit/s TDM transmission of 0.98 ps pulses over 40 km employing dispersion slope compensation," in *Conf. Optic. Fiber Commun. (OFC'96)*, postdeadline paper pd24, San Jose, CA, 1996.
[7] J. A. Salehi, A. M. Weiner, and J. P. Heritage, "Coherent ultrashort light pulse code-division multiple access communication systems," *J. Lightwave Technol.*, vol. 8, pp. 478–491, 1990.
[8] P. R. Prucnal, M. A. Santoro, and T. R. Fan, "Spread spectrum fiber-optic local area network using optical processing," *J. Lightwave Technol.*, vol. 4, pp. 547–554, 1986.
[9] S. Tamura, S. Nakano, and K. Okazaki, "Optical code-multiplex transmission by gold sequences," *J. Lightwave Technol.*, vol. 3, pp. 121–127, 1985.
[10] R. A. Griffin, D. D. Sampson, and D. A. Jackson, "Coherence coding for photonic code-division multiple access networks," *J. Lightwave Technol.*, vol. 13, pp. 1826–1837, 1995.
[11] J. Y. Hui, "Pattern code modulation and optical decoding-A novel code-division multiplexing technique for multifiber networks," *IEEE J. Select. Areas Commun.*, vol. 3, pp. 916–927, 1985.
[12] M. E. Marhic and Y. L. Chang, "Pulse coding and coherent decoding in fiber-optic ladder networks," *Electron. Lett.*, vol. 95, 1535–1536, 1989.
[13] D. Zaccarin and M. Kavehrad, "An optical CDMA system based on spectral encoding of LED," *IEEE Photon. Technol. Lett.*, vol. 4, pp. 479–482, 1993.
[14] D. D. Sampson, G. J. Pendock, and R. A. Griffin, "Photonic code-division multiple access communications," *Fiber Integrated Opt.*, vol. 16, pp. 129–157, 1997.
[15] A. M. Weiner, and J. A. Salehi, "Optical code-division multiple access," in *Photonics in Switching*, J. E. Midwinter, Ed. San Diego, CA: Academic, 1993, vol. 2, pp. 73–118.
[16] J. A. Salehi, "Code division multiple-access techniques in optical fiber networks—Part 1: Fundamental principles," *IEEE Trans. Commun.*, vol. 37, pp. 824–833, 1989.
[17] M. E. Marhic, "Coherent optical CDMA networks," *J. Lightwave Technol.*, vol. 11, pp. 854–864, 1993.
[18] M. Kavehrad and D. Zaccarin, "Optical code-division-multiplexed systems based on spectral encoding on noncoherent sources," *J. Lightwave Technol.*, vol. 13, pp. 534–545, 1995.
[19] L. Nguyen, B. Aazhang, and J. F. Young, "All-optical CDMA with bipolar codes," *Electron. Lett.*, vol. 31, pp. 469–470, 1995.
[20] C.-C. Chang, H. P. Sardesai, and A. M. Weiner, "Code-division multiple access encoding and decoding of femtosecond optical pulses over a 2.5 km fiber link," *IEEE Photon. Technol. Lett.*, vol. 10, pp. 171–173, 1998.
[21] K. Tamura, E. P. Ippen, H. A. Haus, and L. E. Nelson, "77-fs pulse generation from a stretched-pulse modelocked all-fiber ring laser," *Opt.*

Lett., vol. 18, pp. 1080–1082, 1993.
[22] P. Maine, D. Strickland, P. Bado, M. Pessot, and G. Mourou, "Generation of ultrahigh peak power pulses by chirped pulse amplification," *IEEE J. Quantum Electron.*, vol. 24, pp. 398–403, 1988.
[23] A. Galvanauskas, M. E. Fermann, and D. Harter, "High-power amplification of femtosecond optical pulses in a diode-pumped fiber system," *Opt. Lett.*, vol. 19, pp. 1201–1203, 1993.
[24] A. M. Weiner, J. P. Heritage, and J. A. Salehi, "Encoding and decoding of femtosecond pulses," *Opt. Lett.*, vol. 13, pp. 300–302, 1988.
[25] A. M. Weiner, J. P. Heritage, and E. M. Kirchner, "High resolution femtosecond pulse shaping," *J. Opt. Soc. Amer.*, vol. B5, pp. 1563–1572, 1988.
[26] A. M. Weiner, D. E. Leaird, J. S. Patel, and J. R. Wullert, "Programmable shaping of femtosecond optical pulses by use of a 128-element liquid crystal phase modulator," *IEEE J. Quantum Electron.*, vol. 28, pp. 908–920, 1992.
[27] A. M. Weiner, "Femtosecond optical pulse shaping and processing," *Progr. Quantum Electron.*, vol. 3, pp. 161–233, 1995.
[28] R. N. Thurston, J. P. Heritage, A. M. Weiner, and W. J. Tomlinson, "Analysis of picosecond pulse shape synthesis by spectral masking in a grating pulse compressor," *IEEE J. Quantum Elect.*, vol. 22, pp. 682–696, 1986.
[29] R. Kashyap, S. V. Chernikov, P. F. McKee, and J. R. Taylor, "30 ps chromatic dispersion compensation of 400 fs pulses at 100 Gbits/s in optical fibers using an all fiber photoinduced chirped reflection grating," *Electron. Lett.*, vol. 30, pp. 1078–1080, 1994.
[30] M. Stern, J. P. Heritage, and E. W. Chase, "Grating compensation of third order fiber dispersion," *IEEE J. Quantum Electron.*, vol. 28, pp. 2742–2748, 1992.
[31] C.-C. Chang, A. M. Weiner, A. M. Vengsarkar, and D. W. Peckham, "Broadband dispersion compensation for sub-100 fs pulses with a compression ratio of 300," *Opt. Lett.*, vol. 21, pp. 1141–1143, 1996.
[32] C.-C. Chang and A. M. Weiner, "Fiber transmission of sub-500-fs pulses using a dispersion-compensating fiber," *IEEE J. Quantum Electron.*, vol. 33, pp. 1455–1464, 1997.
[33] C. C. Chang, H. P. Sardesai, and A. M. Weiner, "Dispersion-free fiber transmission for femtosecond pulses using a dispersion-compensating fiber and a programmable pulse shaper," *Opt. Lett.*, vol. 23, pp. 283–285, 1998.
[34] A. M. Vengsarkar, A. E. Miller, M. Haner, A. H. Gnauck, W. A. Reed, and K. L. Walker, "Fundamental-mode dispersion compensating fibers: Design considerations and experiments," in *Tech. Dig., Conf. Optic. Fiber. Commun. (OFC' 94)*, paper Thk2, pp. 225–227, 1994.
[35] E. P. Ippen and C. V. Shank, in *Ultrashort Light Pulses*, S. L. Shapiro, Ed. Berlin, Germany: Springer-Verlag, 1984, pp. 83–122.
[36] G. P. Agrawal, *Nonlinear Fiber Optics*, 2nd ed. San Diego, CA: Academic, 1995.
[37] G. P. Agrawal and M. J. Potasek, "Nonlinear pulse distortion in single-mode optical fibers at zero-dispersion wavelength," *Phys. Rev. A.*, vol. 33, pp. 1765–1776, 1986.
[38] M. Stern, J. P. Heritage, W. T. Anderson, and J. Kilmer, "Soliton technique to characterize single-mode fiber dispersion," *J. Lightwave Technol.*, vol. 10, pp. 1777–1779, 1992.
[39] J. P. Gordon, "Theory of the soliton self-frequency shift," *Opt. Lett.*, vol. 11, pp. 662–664, 1986.
[40] J. K. Lucek and K. J. Blow, "Soliton self-frequency shift in telecommunications fibers," *Phys. Rev. A.*, vol. 45, pp. 6666–6674, 1992.
[41] H. P. Sardesai and A. M. Weiner, "Nonlinear fiber-optic receiver for ultrashort pulse code division multiple access communications," *Electron. Lett.*, vol. 33, pp. 610–611, 1997.
[42] ———, "A nonlinear fiber-optic thresholder for spectrally coded ultrashort pulses with 36 dB extinction ratio," *OSA TOPS Ultrafast Electron. Optoelectron.*, vol. 13, 1997.
[43] Z. Zheng, A. M. Weiner, J. H. Marsh, and M. M. Karkhanehchi, "Ultrafast optical thresholding based on two-photon absorption GaAs waveguide photodetectors," *IEEE Photon. Technol. Lett.*, vol. 9, pp. 493–495, 1997.
[44] L. P. Barry, B. C. Thomson, J. M. Dudley, and J. D. Harvey, "Autocorrelation and ultrafast optical thresholding at 1.5 μm using a commercial InGaAsP 1.3 μm laser diode," *Electron. Lett.*, vol. 34, pp. 358–360, 1998.
[45] S. Shen, C.-C. Chang, H. P. Sardesai, V. Binjrajka, and A. M. Weiner, submitted for publication.
[46] M. E. Fermann, V. daSilva, D. A. Smith, Y. Silberberg, and A. M. Weiner, "Shaping of ultrashort pulses by using an integrated acousto-optic tunable filter," *Opt. Lett.*, vol. 18, pp. 1505–1507, 1993.
[47] T. Kurokawa, H. Tsuda, K. Okamoto, K. Naganuma, H. Takenouchi, Y. Inoue, and M. Ishii, "Time-space-conversion optical signal processing using arrayed-waveguide grating," *Electron. Lett.*, vol. 33, pp. 1890–1891, 1997.
[48] J. E. Ford, J. A. Walker, M. C. Nuss, and D. A. B. Miller, "32 channel WDM graphic equalizer," *Tech. Dig., IEEE LEOS 1996 Summer Topical Meetings Broadband Optical Networks*, Keystone, CO, Aug. 1996, pp. 26–27.

H. P. Sardesai, photograph and biography not available at the time of publication.

C.-C. Chang, photograph and biography not available at the time of publication.

A. M. Weiner, photograph and biography not available at the time of publication.